DNA unhooking from a single post as a deterministic process: Insights from translocation modeling

Nabil Laachi, Jaeseol Cho, and Kevin D. Dorfman*
Department of Chemical Engineering and Materials Science, University of Minnesota–Twin Cities, 421 Washington Ave. SE, Minneapolis, Minnesota 55455, USA
(Received 15 December 2008; published 31 March 2009)

Using stochastic methods developed for DNA translocation through nanopores, we study the unhooking of a long DNA chain from an isolated stationary micropost. Such methods quickly and efficiently furnish both the full probability distribution of the unhooking time and the ensuing moments for a wide range of chain and field parameters. The results compare favorably to more realistic but computationally intense Brownian dynamics simulations. For typical chain lengths and applied electric fields used in experiments, the unhooking process is effectively deterministic; diffusive fluctuations make a negligible contribution to the first and second moments of the unhooking time. This result lends credence to continuous-time random-walk models of the overall transport process that treat the unhooking as a convective process.

DOI: 10.1103/PhysRevE.79.031928 PACS number(s): 87.15.Tt, 85.85.+j, 05.40.Jc

I. INTRODUCTION

Gel electrophoresis remains the most widely exploited technique for separating DNA by size [1]. It owes its success to the simplicity of the procedure and the manageability of the equipment involved—all you need is a gel, a voltage source, and a method of detection. However, the technique suffers from a major limitation: while the electrophoretic mobility during biased reptation varies inversely with molecular weight under a range of conditions [1], this dependence breaks down for long molecules [~20 kilobase pairs (kbp)] and/or high fields. More precisely, the mobility saturates to a size-independent value when the chain becomes oriented with the field (biased reptation with orientation) [1,2]. One can circumvent this impediment by periodically switching the direction of the electric field, a method known as pulsed field gel electrophoresis [3]. Typical separations of megabase pair DNA by pulsed field gel electrophoresis are very slow, requiring approximately 1 day to achieve adequate resolution [1,3].

The rise of micro- and nanofluidics has opened a number of promising avenues toward addressing the limitations of gel electrophoresis for DNA separations [1]. Various devices have recently emerged, benefiting greatly from advances in fabrication techniques [4–6]. We focus here on the use of artificial "gels" created by periodic arrays of cylindrical obstacles. Early experiments [7] demonstrated the potential of this method for separating DNA in the tens to hundreds of kilobase pair range. Subsequently, Kaji *et al.* [8] successfully separated λ-DNA (48.5 kbp) and T4-DNA (168.9 kbp) within 10 s in a quartz chip containing nanopillars of diameter and spacing 500 nm without using a pulsed field technique. Similarly, Viovy and co-workers reported rapid separations of various DNA sizes in magnetic matrices with bead columns of size 1–5 μm and spacing 3–10 μm [9,10]. These separations require minutes, a 1000-fold improvement over pulsed field gel electrophoresis.

While the reptation concept can no longer be applied in the case of the dynamics of DNA chains in sparse arrays of posts [1], the simple mechanical description of the post collision as unhooking by a rope-over-pulley motion, first proposed by Volkmuth *et al.* [11], has been used extensively [12–16]. In this approach, a deterministic force balance leads to a logarithmic size dependence of the unhooking time of the chain [11,13,14]. Inspired by the geometration model of DNA migration through stationary networks of obstacles [17–20], Minc *et al.* [13] expanded upon this simple rope-over-pulley picture to build a somewhat more complex microscopic model of DNA motion in arrays of posts. Their application of continuous-time random-walk (CTRW) theory to the model led to analytical expressions for the mean velocity through the array and the dispersion characterizing the broadening of the bands [13]. The model was subsequently modified to take into account moderate magnitudes of the electric field and their effect on chain extension during the collision [21–23].

While this CTRW model captures the qualitative aspects of the transport properties of DNA through the post array, developing a quantitatively accurate model of the effective diffusion (dispersion) coefficient of long DNA requires a more fundamental understanding of the elementary problem of collision and unhooking from a single post. Importantly, the CTRW models [13,21,23] assume that the dispersion arises solely from the random offset between the two arms and the random distance between collisions. The deterministic rope-over-pulley model used to quantify the unhooking time possesses a singularity (divergence of the total hold-up time) when the two arms are of equal length after unraveling around the post. If one includes diffusive fluctuations in the unhooking model, the singularity can be removed [11,12]. However, incorporating such fluctuations into the extant CTRW theories [13] for migration through an array is not trivial. Our goal here is to study these fluctuations and determine whether they play an important role in experiments and therefore need to be included in the CTRW model.

The present contribution thus focuses on the first-passage time statistics for the unhooking of a long DNA molecule on

*dorfman@umn.edu

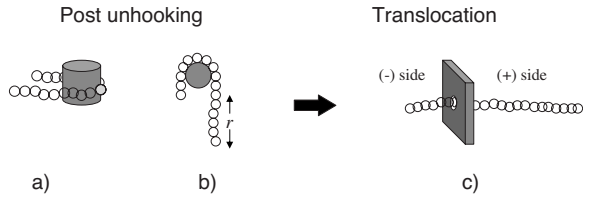

FIG. 1. (a) Side view of DNA chain with extended arms unhooking from a cylindrical obstacle. (b) Top view of the same chain. (c) Translocation of the polymer through a narrow hole in an impenetrable membrane. The parameter r represents the instantaneous offset between the lengths of the two arms.

a cylindrical post in a dc field. In our analysis, we would like to avoid computational issues inherent in the Fokker-Planck model [11] and Brownian dynamics (BD) [12] simulations used previously. In what follows, we show how the unhooking of a DNA chain can be mapped to a translocation problem. As illustrated in Fig. 1, if one neglects the size of the insulating post and the curvature of the electric field lines it induces, the two extended arms can be envisioned as being situated on two sides of an impenetrable "membrane." In Sec. III B, we will assess the validity of these assumptions. Transfer of mass between arms occurs only through a narrow opening in the membrane under the action of a well-defined force that depends on the difference in length between the arms. When viewed in this light, the unhooking process can be analyzed using the plethora of methods developed for DNA translocation through nanopores [24–27].

At this point in our discussion, we would like to stress that the analogy between the translocation of a chain through a nanopore and the unhooking from a post lies in the methods utilized to characterize the two motions rather than the actual physical mechanisms underlying these processes. Chains translocating through a nanopore are pulled via the combination of entropic elasticity and an external force (an electric field or a chemical-potential difference), while the chain disengages from the post under the action of an electric field. Nevertheless, both processes can be described as the biased motion of a one-dimensional (1D) Brownian particle in a well-defined potential field, governed by the free energy of the chain on either side of the membrane. In characterizing such motion, the value of the total force driving the chain will prove more relevant than its actual physical nature.

We thus have two goals in the present contribution: (i) We will demonstrate that simple and efficient translocation models furnish excellent agreement with results obtained using the Fokker-Planck equation and BD simulations. (ii) We will take advantage of this computational efficiency to study the long chains used in experiments over a wide range of electric fields and initial configurations. Taken together, these two results will allow us to provide support for CTRW models of the transport in an array that incorporate a deterministic rope-over-pulley unhooking model. Before embarking on this task, it is useful to first recall the various methods we can use to analyze the unhooking process.

II. ANALYSIS METHODS

In what follows, we investigate the unhooking of a single DNA chain wrapped around an isolated fixed cylindrical obstacle. The equally important problems of chain collision and translation in an array of posts are not considered in the present analysis; these problems are often treated separately [13,20]. We only consider "U"- and "J"-shaped collisions where the unraveling and unhooking processes can be decoupled. This decoupling is essential to the partially separable probability distribution function invoked to describe the motion of the chain in an array [13]. Previous results from Randall and Doyle [14] indicated that unraveling and unhooking of the chain are sometimes coupled (the so-called X collision). However, an effective J model with a shortened chain adequately describes the X collisions observed in experiments [14].

We model the DNA as a polymeric chain of total charge Q and contour length $L=Nl_p$, where N is the number of persistence lengths of size l_p. The parameters N and l_p are chosen to reflect typical experimental situations. For double-stranded DNA, $l_p \sim 53$ nm (or 150 bp) and typical experiments use DNA of size $N \sim 50-500$. Upon collision with the stationary post, two well-defined "arms" are formed on either side of the post. The applied electric field of magnitude E leads to an external tension (which favors stretching) that exceeds the entropic energy (which favors coiling) [28]. As a result of the excess external tension, the coiled arms of the chain extend on either side of the post to near to their full contour length, giving rise to U- and J-shaped conformations. This simple picture is supported by experimental evidence on DNA molecules tens of micrometers long, which can be extended under the action of electric fields as low as 1 V/cm [11]. In our analysis, we focus on electric fields $E \sim 5-50$ V/cm. In terms of the dimensionless Péclet number (to be defined below), $\mathrm{Pe} \sim 0.1-1$.

Our starting point is a chain enveloping a post with fully extended arms and an initial configuration defined by an offset $-L \leq x_0 \leq L$ between the two arms. An offset of $x_0=0$ corresponds to a chain with equal arms, while an offset of $x_0=\pm L$ represents a chain fully located on one side of the post. The diffusive motion, combined with the convection due to the electric field, causes the chain to sway back and forth around the post in a rope-over-pulley manner until the longer arm eventually engulfs its smaller counterpart. A full description of the motion of the polymer can be obtained via the probability distribution function of the exit (or unhooking) time, i.e., the time necessary for the entire mass of the chain to reside on one side of the post. This time is a function of the initial offset, the field, and the chain properties. Taking advantage of the parallel between the unhooking problem and the translocation of a chain, the probability distribution function and the moments of the exit times can be computed using the methods outlined below.

A. Fokker-Planck approach

The rope-over-pulley collision was originally analyzed using a Fokker-Planck (FP)-type equation [11], and equivalent models of translocation have also appeared [24,25]. In this approach, the probability $p \equiv p(x,t)$ for the chain to exhibit an offset x at time t is governed by a convection-diffusion equation of the form

$$\frac{\partial p}{\partial t} = D\frac{\partial}{\partial x}\left[\frac{\partial p}{\partial x} + \frac{\partial U(x)}{\partial x}p\right]. \tag{1}$$

In the latter, D is the free-solution diffusion coefficient of the chain and, for the post collision, $U(x)=-QEx^2/2L$ is the inverted harmonic electric potential engendered by the offset between the two arms [11]. The governing equation for p is supplemented with the absorbing boundary conditions at $x=\pm L$, $p(\pm L,t)=0$, as well as the initial condition $p(x,0)=\delta(x_0)$.

Let us introduce the following dimensionless parameters:

$$\mathrm{Pe} \equiv \frac{qEl_p}{k_BT}, \quad \tau \equiv \frac{t}{t_p}, \quad r \equiv \frac{x}{l_p}, \quad r_0 \equiv \frac{x_0}{l_p}, \tag{2}$$

where Pe is the Péclet number, k_BT is the thermal energy, $q=Q/N$ is the charge per persistence length, and $t_p=l_p^2/2D_0$ is the diffusion time of a persistence length with a diffusion coefficient of $D_0=ND$. The latter scaling implies Rouse dynamics for the diffusion of this highly stretched chain, consistent with the conclusions of André *et al.* [29]. The governing equation for p in Eq. (1) becomes

$$\frac{\partial p}{\partial \tau} = \frac{2}{N}\frac{\partial}{\partial r}\left(\frac{\partial p}{\partial r} + \frac{\mathrm{Pe}}{2}rp\right), \tag{3}$$

subject to the boundary conditions

$$p(-N,\tau) = p(N,\tau) = 0 \tag{4}$$

and the initial condition

$$p(r,0) = \delta(r_0). \tag{5}$$

The survival probability, i.e., the probability that the chain still remains hooked at time τ, is given by

$$S(\tau) = \int_{-N}^{N} p(r,\tau)dr. \tag{6}$$

The probability distribution $\Pi \equiv \Pi(\tau)$ for observing an exit event before time τ can thus be expressed as

$$\Pi(\tau) = -\frac{dS}{d\tau}. \tag{7}$$

With the latter, the nth moment of the exit time, $\langle \tau_e^{(n)} \rangle$, is given by

$$\langle \tau_e^{(n)} \rangle = \int_0^{\infty} \tau^n \Pi(\tau)d\tau. \tag{8}$$

Using the above notation and electric potential, the average exit time (or mean first passage time), $\langle \tau_e \rangle \equiv \langle \tau_e^{(1)} \rangle$, can be explicitly calculated by [11,30]

$$\langle \tau_e(r_0) \rangle = \frac{2N}{\mathrm{Pe}}\int_0^{\infty} \frac{e^{-4y^2}}{y}\sin[\lambda y(1-r_0)]\sin[\lambda y(1+r_0)]dy, \tag{9}$$

where $\lambda \equiv N\sqrt{\mathrm{Pe}}$.

Note that this expression does not entail any singularities when the two arms are initially of equal length, i.e., $r_0=0$. Indeed, if $r_0=0$, the net force on the chain is zero; it is in an unstable state, sitting on top of the inverted harmonic potential. As thermal fluctuations will inevitably push the chain, even slightly, away from that position, the resulting nonzero electrical force leads to the chain unhooking in a finite time.

Using this Fokker-Planck approach, Volkmuth *et al.* [11] compared the average exit time given by the above expression to experimental results on the unhooking of a chain from a single post. While the closed-form expression of the average exit time in Eq. (9) makes the Fokker-Planck approach attractive at first sight, no closed-form expression for Π or its higher moments is available. Thus, numerical manipulation of Eqs. (3), (6), and (7) becomes necessary to obtain information about the variance of the unhooking times. As soon as the number of persistence lengths N exceeds a few hundred, accurate solutions necessitate smaller and smaller discretization steps to numerically integrate Eq. (3). Although feasible, the computationally intense numerical integration constitutes a major limitation of this method. In the discussion below, we show how the entire probability distribution of the exit time and its moments can be calculated without solving for $p(r,\tau)$.

B. Monte Carlo simulations

Gauthier and Slater [27] devised a simple calculation method to compute the probability distribution Π of the exit time τ_e of a chain translocating through a nanopore, which we will adapt to the problem at hand. This method is of particular interest here because it is simple, fast, and efficient, as one need not resort to a numerical integration of the partial differential equation in Eq. (3) and its solution $p(r,\tau)$ to obtain Π. In this algorithm, the motion of the chain during the translocation process is modeled as a series of discrete jumps between the positive and negative sides of the membrane used to model the steric effect of the post. The chain proceeds accordingly from one side to the other by diffusion and electric field-induced convection until all the segments reside on the same side. If $n_{\pm}$ is the number of segments on the $\pm$ side of the post depicted in Fig. 1, the chain diffuses in an electric potential $U/k_BT=-\mathrm{Pe}(n_+-n_-)^2/4$. The force F acting upon the chain is thus

$$F = -\frac{1}{l_p}\frac{\partial U}{\partial n_+} \tag{10}$$

or, in dimensionless form,

$$\epsilon \equiv \frac{Fl_p}{2k_BT} = \frac{\mathrm{Pe}}{2}(n_+ - n_-) = \frac{\mathrm{Pe}}{2}(2n_+ - N). \tag{11}$$

At every time step of the translocation process, the chain motion is that of a 1D Brownian particle in the potential U between two absorbing walls. Starting halfway between the walls, the particle undergoes a biased random walk until it is absorbed by one of the two walls after a finite time Δt. In other words, the chain will "jump" either to the right (+) or to the left (−) configuration with a probability p_+ or p_- in an average time Δt. However, this simple description is incomplete. In order to retrieve the correct mobility and diffusion

coefficient, one must also consider cases where the chain does not perform a jump during Δt, but rather remains in the same configuration [31]. Time steps without a jump are necessary to correctly simulate the biased random walk using constant time steps and calculate its transport properties.

Our goal here is not to dwell on the details of the algorithm; these are well-described elsewhere [27,31,32]. Rather, we present the main characteristics, namely, the jump probabilities and the corresponding time step. We consider then a chain initially distributed such that $n_+ - n_- = r_0$. Under the action of the force ϵ, the chain jumps to the $+/-$ configuration with the probabilities [27]

$$p_\pm = \frac{1 - s(\epsilon)}{1 + e^{\mp 2\epsilon}} \tag{12}$$

or remains at rest with the probability [27]

$$s(\epsilon) = \frac{\coth \epsilon}{\epsilon} - \operatorname{csch}^2 \epsilon \tag{13}$$

during the dimensionless time [27]

$$\Delta t(\epsilon) = [1 - s(\epsilon)] \frac{\tanh \epsilon}{\epsilon} t_b'. \tag{14}$$

In the latter, $t_b' = N$ takes into account the frictional effects during the motion of the chain [27].

The algorithm proceeds and time is updated until $n_+ = 0$ or N, hence obtaining one realization of the exit time τ_e. The probability distribution Π can thus be generated using multiple runs of the random-walk simulation starting at the same initial offset.

C. Master-equation approach

If one is interested in obtaining moments of the exit time for different initial configurations, one must generate ensembles of Monte Carlo (MC) calculations for each of the desired initial configurations. While certainly feasible, this is not computationally efficient. Such difficulty can be circumvented if one resorts to a master-equation (ME) formulation approach [26], which was also developed for translocation by Gauthier and Slater [27]. Here, the chain, modeled as a series of N segments subject to the force ϵ, can be found at each particular time step in any of $N+1$ possible configurations. The configurations are defined by the excess (or deficit) number of segments on the positive side of the membrane. Let P_+^i and P_-^i denote the probabilities to escape on the positive and negative sides, respectively, given that the chain starts at some configuration $1 \le i \le N+1$; $i \equiv n_+ + 1$ such that $i=1$ corresponds to a chain escaping on the negative side and $i=N+1$ to a chain escaping on the positive side.

Using a master-equation approach, a chain in configuration $2 \le i \le N$ at a particular point in time will assume a configuration $(i-1, i, i+1)$ at the next time step. The corresponding transition probabilities are (p_-, s, p_+). The escape probabilities $P_\pm^i$ can thus be calculated using the tridiagonal system [27]

$$P_\pm^i = p_+^i P_\pm^{i+1} + s^i P_\pm^i + p_-^i P_\pm^{i-1}, \tag{15}$$

where $p_\pm^i$ and s are defined in Eq. (12) for each configuration i. The absorbing boundary conditions when the polymer is entirely located on either side ensure that $P_+^1 = 0, P_+^{N+1} = 1$ and $P_-^1 = 1, P_-^{N+1} = 0$. Note that since all chains ultimately exit through one of the two sides for any given initial configuration i, we must have $P_+^i + P_-^i = 1$.

The mean exit times $\tau_\pm^i$ through the $\pm$ side are obtained by solving well-defined tridiagonal systems [27]. However, interest lies here in the average time $\langle \tau_e^i \rangle = P_+^i \tau_+^i + P_-^i \tau_-^i$ to exit on either side. Combining the equation for $\tau_\pm$ and $P_\pm$, one arrives at the following system for $\langle \tau_e^i \rangle$:

$$\langle \tau_e^i \rangle = p_+^i \langle \tau_e^{i+1} \rangle + s^i \langle \tau_e^i \rangle + p_-^i \langle \tau_e^{i-1} \rangle + \Delta t^i. \tag{16}$$

The average exit time of a chain with a configuration i at a particular step is thus equal to the weighted average exit time to escape starting at adjacent configurations $(i-1, i, i+1)$ at the next step, augmented by the time elapsed during the step, Δt^i. The previous system is supplemented by the boundary conditions $\langle \tau_e^1 \rangle = \langle \tau_e^{N+1} \rangle = 0$.

One can repeat this procedure to compute higher moments of τ_e. For the sake of completeness, we provide the tridiagonal system to be solved for the second moment $\langle \tau_e^{i(2)} \rangle$:

$$\langle \tau_e^{i(2)} \rangle = p_+^i \langle \tau_e^{i+1(2)} \rangle + s^i \langle \tau_e^{i(2)} \rangle + p_-^i \langle \tau_e^{i-1(2)} \rangle + \langle \tau_e^i \rangle^2 - (\langle \tau_e^i \rangle - \Delta t^i)^2, \tag{17}$$

supplemented by $\langle \tau_e^{1(2)} \rangle = \langle \tau_e^{N+1(2)} \rangle = 0$. The standard deviation σ of the exit time is thus given by

$$\sigma = \sqrt{\langle \tau_e^{i(2)} \rangle - \langle \tau_e^i \rangle^2}. \tag{18}$$

The enthusiasm raised by this rapid procedure of calculating the moments of the exit time for all possible initial configurations in one single calculation should nevertheless be tempered by the fact that one can only obtain the moments of the exit time, rather than the full probability distribution Π of the exit time. However, several techniques [33] can be used to build an approximation of Π from its moments. We do not engage in such a task though, since the exact distribution is readily available from the previously outlined Monte Carlo algorithm.

D. Brownian dynamics simulations

In order to compare results from MC and ME calculations, we also implemented a BD simulation code. The particular algorithm outlined here has appeared elsewhere [34]. Our BD simulations employ a bead-spring model with a chain of contour length L represented by N_b beads connected by $N_s = N_b - 1$ springs. Each spring contains $\nu = l_s / l_p$ persistence lengths, where l_s is the maximum extension of a spring and l_p is the persistence length of DNA. The total number of persistence lengths (or, equivalently, MC beads) is therefore $N = \nu N_b$.

The position of each bead, $\mathbf{r}_i$, obeys the following equation of motion [34]:

$$\frac{d\mathbf{r}_i}{dt} = -\mu_0 \mathbf{E}(\mathbf{r}_i) + \frac{1}{\zeta}(\mathbf{F}_i^B + \mathbf{F}_i^{\mathrm{EV}} + \mathbf{F}_i^T), \tag{19}$$

where μ_0 is the bead electrophoretic mobility and ζ is the bead drag coefficient. Exact expressions for the components of the electric field, $\mathbf{E}$, as a function of the bead position can be obtained analytically by conformal mapping [35]. The Brownian force, $\mathbf{F}^B$, is computed from a Gaussian distribution with zero mean and correlation

$$\langle \mathbf{F}_i^B(t_1)\mathbf{F}_j^B(t_2)\rangle = \frac{2k_BT\zeta\delta_{ij}}{\delta t}\mathbf{I}, \tag{20}$$

where δ_{ij} is the Kronecker delta function, δt is the time step, and $\mathbf{I}$ is the unit tensor. The excluded volume force, $\mathbf{F}^{\mathrm{EV}}$, is derived from the gradient of the soft potential developed by Jendrejack *et al.* [36]

$$U^E(r_{ji}) = \frac{1}{8}v^{\mathrm{EV},p}k_BT\nu^2\left(\frac{9\nu}{4\pi l_s^2}\right)^{3/2}\exp\left(-\frac{9\nu r_{ji}^2}{4l_s^2}\right), \tag{21}$$

where $r_{ji}=|\mathbf{r}_i-\mathbf{r}_j|$ and $v^{\mathrm{EV},p}=0.0004\ \mu\mathrm{m}^3$ [34] is the excluded volume of a bead. Each bead is also subject to a tension force, $\mathbf{F}^T$, that results from the flexibility of the adjacent springs. For a wormlike chain, the force, $\mathbf{f}_{i,j}^s$, acting on bead i from the spring connecting adjacent beads i and $j=i+1$ or $j=i-1$ obeys the Marko-Siggia spring force [37]

$$\mathbf{f}_{i,j}^s = \frac{k_BT}{A_{\mathrm{eff}}}\left[\frac{r_{ji}}{l_s} - \frac{1}{4} + \frac{1}{4(1-r_{ji}/l_s)^2}\right]\frac{\mathbf{r}_j-\mathbf{r}_i}{r_{ji}}. \tag{22}$$

The parameter A_{eff} denotes the effective persistence length, which is determined by a wormlike chain model with the Underhill-Doyle low-force criteria [38]. The tension force, $\mathbf{F}_i^T$, on each inner bead is thus the sum of the two adjacent spring forces, whereas, for the two end beads, it is given by the force from the one adjacent spring.

In the simulations, the force balance given by Eq. (19) is nondimensionalized using appropriate length, time, and force scales for a BD model. Since the motion of the chain can only be resolved down to the spring length scale in BD, we choose the maximum extension of the spring, $l_s=\nu l_p$, as a characteristic length. Likewise, if $D_s=D_0/\nu$ is the diffusion coefficient of a spring composed of ν persistence lengths of diffusion coefficient D_0, then the diffusion time of a spring, $t_s \equiv l_s^2/2D_s=\nu^3 t_p$, is a proper characteristic time scale for the motion of the chain. Following Kim and Doyle [34], the electric force can be expressed in a dimensionless form as $F_s \equiv \mu_0 E l_s/D_s=\nu^2\mathrm{Pe}$.

Note that these definitions of the motion characteristic scales differ from those introduced previously in Eq. (2) for MC and ME calculations. In the former, the spring constitutes the elementary unit of the chain, while in the latter, all quantities are defined relative to a persistence length, considered to be the elementary unit.

The equation of motion in Eq. (19) is integrated using an adaptive method [34]. The interaction between the beads and the post (nonpenetrability) is enforced using the Heyes-Melrose algorithm [34,39]. Due to the presence of $\mathcal{O}(1)$ gradients of the electric field near the post, small time steps are required to achieve an adequate resolution of the motion of the beads there, resulting in a high computational cost.

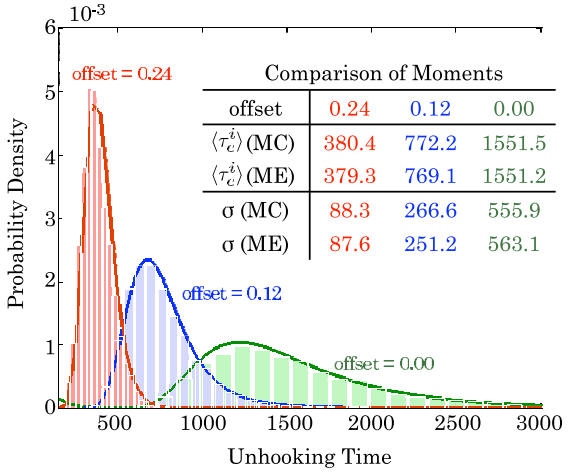

FIG. 2. (Color online) Probability distribution of the exit time for several fractional initial offsets. An initial offset of zero corresponds to two equal arms and an offset of one represents a chain fully located on one side of the post. The histograms are obtained from the MC algorithm and the solid lines from the Fokker-Planck equation in Eq. (7). Inset shows comparisons of the average $\langle \tau_e^i \rangle$ and standard deviation σ of the exit time calculated using the MC and ME methods.

In our simulations in Sec. III B, we represent a chain $L=10.25\ \mu$m long, with $N_b=29$ Brownian beads (or $N\sim 194$ persistence lengths), leading to a maximum spring extension $l_s=366.1$ nm. This chain length represents half the contour length of stained λ-DNA. To initialize the chain, the 15th bead is placed at the center of the backside of an infinitely extended cylindrical obstacle of diameter $d=1\ \mu$m. The other beads are distributed symmetrically around the obstacle with a spacing equal to the equilibrium spring length, $\sqrt{\nu}l_p$. Upon reaching an angle of $\pm\pi/2$ along the obstacle contour, any remaining beads are placed with the same spacing $\sqrt{\nu}l_p$ in the direction of the nominal electric field. We found that simulations starting from this symmetric state are very sensitive to the number of beads used to represent the chain, but a choice of 29 beads yields satisfactory results.

III. RESULTS AND DISCUSSION

A. Influence of diffusion

We first demonstrate the consistency of the unhooking probability distribution and moments of that distribution obtained using the Fokker-Planck, Monte Carlo, and master-equation methods. For this purpose, we consider a chain composed of 50 beads, thus corresponding to a total contour length of about 7.5 kbp. The chain, wrapped around the post, can unhook through the combined action of diffusion and the electric force. The Péclet number, $\mathrm{Pe}=0.1$, corresponds to $E\sim 5$ V/cm. Figure 2 presents the probability distribution of the exit time for various initial offsets between the two extended arms of the chain. The histograms are obtained from 50 000 realizations of the exit time using the Monte Carlo algorithm described above, while the solid lines correspond

to the numerical integration of the Fokker-Planck approach. As can be seen from the figure, the discrete MC approach yields a distribution in accordance with the continuous FP approach. The table in the inset of Fig. 2 compares the average and standard deviation of the exit time computed using the MC and ME methods. Here too, the agreement between the ensemble averages of the MC calculations and the exact ME method is very good for all initial offsets. Thus, we will proceed with the ME approach to compute the moments, owing to its computational efficiency. For subsequent comparisons between the present approach and unhooking time distributions obtained by Brownian dynamics simulations, we will use the MC approach.

In addition to illustrating the concordance between the methods, Fig. 2 illuminates the role of the initial offset on the exit time. As the initial offset decreases, the peak of the exit time probability distribution is shifted toward increasing values of time, meaning a slower unhooking process. This shift is accompanied by a broadening of the probability distribution, indicating an increase in the exit time fluctuations.

Both effects are understood by recalling that the driving force is proportional to the difference between the lengths of the two arms, as given by Eq. (11). Accordingly, for small offsets, diffusive effects (responsible for broadening of the distribution) become important since the convective driving force (responsible for the location of the peak) is reduced. The critical offset value, N_c, at which the two effects are comparable in magnitude can be estimated if we consider the point at which convection and diffusion are balanced [15]. The characteristic time for a chain of size N to diffuse over a distance $N_c a$ is

$$t_d \sim \frac{N_c^2 a^2}{D_0/N} \sim N N_c^2, \tag{23}$$

while the convective time scale for the same chain subject to a force $F \sim N_c \mathrm{Pe}$ is

$$t_c \sim \frac{N_c a}{F/\xi} \sim \frac{N_c}{N_c \mathrm{Pe}/N} \sim \frac{N}{\mathrm{Pe}}. \tag{24}$$

Balancing the two time scales, we arrive at the condition

$$\lambda^2 = N_c^2 \mathrm{Pe} \sim 1. \tag{25}$$

This situation is reminiscent of a fluid boundary layer near a flat plate where viscous (diffusive) effects are non-negligible while the flow beyond the boundary layer is purely inertial (convective). This analogy can be extended to the thickness δ of the boundary layer as a function of the Reynolds number (or driving force), $\delta \sim 1/\sqrt{\mathrm{Re}}$, or its equivalent in our case, $N_c \sim 1/\sqrt{\mathrm{Pe}}$.

The parameter $\lambda \equiv N\sqrt{\mathrm{Pe}}$ is thus critical in that it distinguishes between two regimes: for $\lambda^2 \ll 1$, the chain unhooking is governed by diffusive effects; for $\lambda^2 \gg 1$, the chain moves deterministically under the action of the electric field. This distinction is further highlighted in Fig. 3. Here, we plot the rescaled average and standard deviation of the exit time as a function of the initial offset for different Pe. The plot also contains the deterministic exit time obtained from a logarithmic rope-over-pulley model. Note that the standard

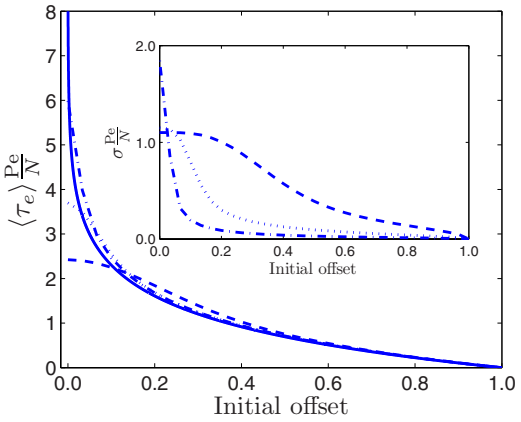

FIG. 3. (Color online) Plot of the rescaled average exit time $\langle \tau_e \rangle \mathrm{Pe}/N$ as a function of the initial offset between the two arms for various Péclet numbers, Pe=0.02 (– –), Pe=0.2 (···), and Pe=2 (–·–) and a value of N=60. The average exit time was obtained using a ME calculation and compared to the deterministic rope-over-pulley model (solid line). Inset shows the variations of the standard deviation of the exit time, also scaled with Pe/N.

deviation in the deterministic case is identically zero. As expected, the impact of diffusive fluctuations is strongest when the initial offset is zero. The purely deterministic model incurs a singularity at this point, since it does not include a mechanism to break the symmetry. As anticipated from the argument above, both the mean unhooking time and its standard deviation decrease as the initial offset increases because the process becomes more and more deterministic. Importantly, as the offset increases, the rescaled average exit time $\langle \tau_e \rangle \mathrm{Pe}/N$ lines collapse onto the deterministic, purely convective curve. Note that as Pe is increased, the collapse occurs for smaller values of initial offset, as dictated by the condition $N_c \sim 1/\sqrt{\mathrm{Pe}}$. We tried to verify the scaling in Eq. (25) by plotting a critical initial offset N_c as a function of Pe. Unfortunately, the value of N_c proved very sensitive to the criterion defining the transition zone.

B. Comparison with Brownian dynamics

While we have demonstrated the consistency between the Fokker-Planck, Monte Carlo, and master-equation stochastic methods outlined above, one might legitimately inquire about the validity of the assumptions underlying the transport model used in these calculations. More specifically, the results we presented above rely on three key assumptions: (i) The chain flexibility was ignored. Rather, both arms were assumed to be completely stretched upon collision with the post; (ii) The post has a vanishing diameter. The experiments cited at the outset [7–10] typically use post diameters commensurate with the radius of gyration of the chain; (iii) The electric field was assumed to be uniform. In typical experiments, the insulating post generates field nonuniformities, both in magnitude and direction, in the vicinity of the post. These field gradients can cause lateral displacements of the chain that are not taken into account in our models.

To test the validity of our assumptions, more realistic Brownian dynamics simulations were performed to study the

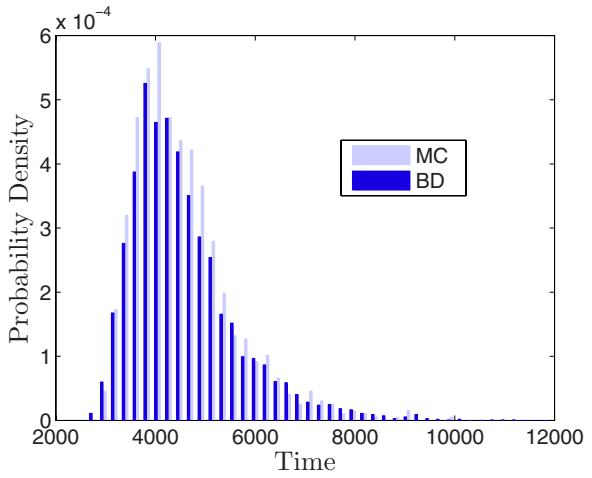

FIG. 4. (Color online) Probability distribution of the exit time of a chain with $N=194$ Monte Carlo beads using an electric field Pe $=0.21$. The chain has initially a zero offset between the arms. The histograms are the results of BD simulations and MC calculations. The two distributions share the same features, namely, the shape, the peak position, and the width of the distribution.

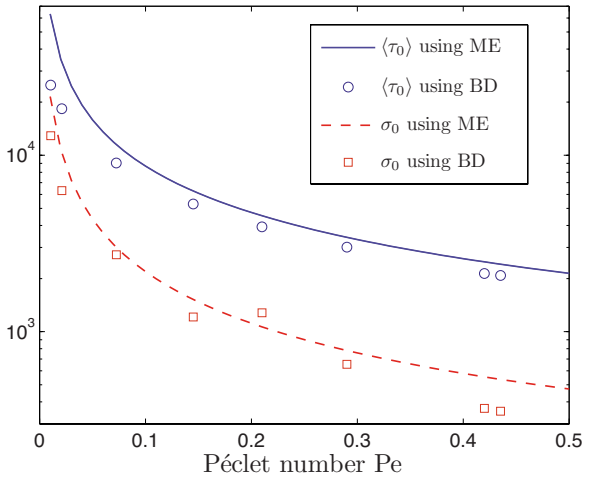

FIG. 5. (Color online) Plots of the average $\langle \tau_0 \rangle$ and standard deviation σ_0 of the exit time of a chain ($N=194$) starting with equal arms. Both quantities are computed from BD simulations and a ME calculation.

chain unhooking problem. As mentioned earlier, our comparison with the Brownian dynamics simulations corresponds to the unhooking of a 10.25 μm chain (or $N \sim 194$ persistence lengths) using a nominal electric field of 10 V/cm (or Pe ~ 0.21). Figure 4 compares the probability distribution of the exit time obtained from the BD simulations and the MC calculation. The BD histograms are the result of 1000 runs of the simulation and the MC bars are obtained from 5000 realizations of the exit time.

The agreement between the two methods is very good given the limited number of computationally expensive BD simulation runs. Qualitatively, the two distributions exhibit identical features (shape, peak position, and width of the distribution). To further investigate the quantitative agreement, we plot in Fig. 5 the average, $\langle \tau_0 \rangle \equiv \langle \tau_e \rangle_{r_0=0}$, and standard deviation, $\sigma_0 \equiv \sigma_{r_0=0}$, of the exit time for the same chain as a function of the Péclet number. The BD data in this figure correspond to 100–300 simulations at each value of the Péclet number. As can be seen from the figure, the agreement between the fast ME calculation and the much slower BD simulation is very satisfying, in particular for the average exit time. The discrepancies of the standard deviation can be improved with more simulation runs, albeit at a high computational cost. The previous results from Figs. 4 and 5 validate our assumptions in modeling the chain. The flexibility of the chain barely affects the escape process and one can neglect the electric field nonuniformities with minimal loss of accuracy. When evaluating the transport coefficients of the unhooking chain, one can thus resort to fast, easily implemented, stochastic methods that perform as well as time-consuming, complex BD simulations.

C. Offset-averaged behavior

Having now established the consistency and accuracy of these translocation methods, we would like to use them to gain insights into experimentally relevant parameter ranges. To aid in the analysis, let us introduce now the random variable $\bar{\tau}_e$ defined as the "mean exit time" or the average of the exit times corresponding to uniformly distributed initial offsets. Nixon and Slater [12] previously considered both uniform and Gaussian distributions of initial offsets in a simpler model and concluded that the choice of distribution has little effect on the scaling behavior of the exit times [12]. If M_0 is the number of possible offsets, then the nth moment of $\bar{\tau}_e$ can thus be obtained by

$$\langle \bar{\tau}_e^{(n)} \rangle = \frac{1}{M_0} \sum_{i=1}^{M_0} \langle \tau_e^{i(n)} \rangle. \tag{26}$$

We can therefore write for the average of $\bar{\tau}$,

$$\langle \bar{\tau}_e \rangle = \frac{1}{M_0} \sum_{i=1}^{M_0} \langle \tau_e^{i} \rangle, \tag{27}$$

and standard deviation

$$\bar{\sigma} = \sqrt{\langle \bar{\tau}_e^{(2)} \rangle - \langle \bar{\tau}_e \rangle^2}. \tag{28}$$

The rescaled $\langle \bar{\tau}_e \rangle$ and $\bar{\sigma}$ are plotted in Fig. 6 as a function of chain length N for various values of Pe. Both $\langle \bar{\tau}_e \rangle$ and $\bar{\sigma}$ saturate to the deterministic value N/Pe [10] after a "boundary layer" zone of size $N_c \sim 1/\sqrt{\mathrm{Pe}}$, explaining why the saturation occurs earlier for high values of Pe. Also, both the average and standard deviation of the mean exit time overshoot their saturation values for small values of N. This should not appear very surprising if one recalls that the zero offset exit time dominates the summation for $\bar{\tau}_e$. For small values of N and a zero initial offset, diffusive fluctuations dominate the early stages of the unhooking, thus leading to an averaged exit time greater than its saturation (deterministic) value. This overshoot was already apparent from Fig. 3, where $\langle \tau_0 \rangle \mathrm{Pe}/N \approx 6$ and $\sigma_0 \mathrm{Pe}/N \approx 2$ for a value of Pe$=2$. Note that the average and standard deviation of the exit time over all uniformly distributed initial offsets for the determin-

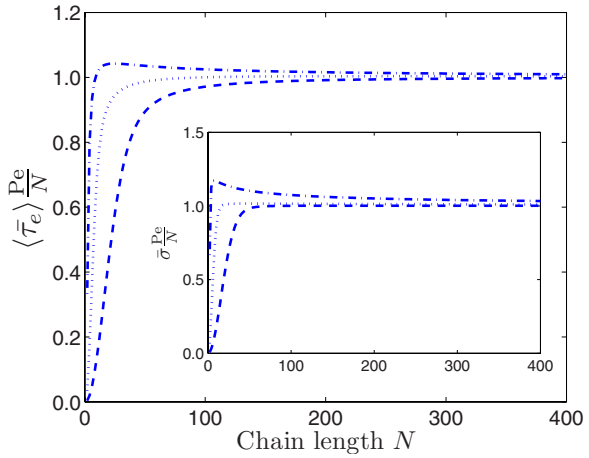

FIG. 6. (Color online) Plot of the rescaled average "mean exit time" $\langle \bar{\tau}_e \rangle$ Pe/N as a function of the chain length N for various Péclet numbers, Pe=0.01 (– –), Pe=0.1 (···), and Pe=1 (–·–). The mean exit time is obtained by averaging the exit time τ over all possible initial offsets. Inset shows the same calculation for the standard deviation of the mean exit time.

istic rope-over-pulley model are N/Pe (the singularity at zero initial offset is integrable [12]), independent of N or Pe [10]. In other words, in the high Péclet regime, the diffusive fluctuations of the chain are negligible and the chain behaves deterministically. In the language of fluid mechanics, the flow is uniform everywhere with no boundary layer.

In experiments, one typically deals with chains several micrometers long ($N \sim 200-500$) animated by an electric field of about 10 V/cm ($\mathrm{Pe} \sim 0.2$). Figure 6 indicates that, for this range of N and Pe, the transport properties of the chain when it disengages from the post are dominated by convective effects; both the mean and standard deviation of the exit time saturate to their deterministic, diffusion-free, limits well before the experimental regime is reached. The result above lends credence to one of the main assumptions underlying the CTRW model discussed at the outset. In this model, the diffusive fluctuations of the chain upon collision are neglected. The dispersivity of the chain mainly arises due to differences in the initial offset between the arms, as well as variations in the distance traveled by the chain between collisions. Including the diffusive fluctuations in the CTRW model should, therefore, only affect the transport coefficients of the chain for a limited range of N and Pe, corresponding to the condition $\lambda^2 \ll 1$. Consequently, treating the unhooking process as a purely convective process is a valid assumption.

IV. CONCLUSION

We have explored the problem of chain unhooking from a post using stochastic methods developed for DNA translocation through a nanopore. We have shown how these methods can be implemented to obtain the probability distribution of the unhooking time and its moments in a fast and efficient way, thereby establishing the consistency between the various methods. The Monte Carlo method provides the full probability distribution for a given initial offset, while the master-equation approach leads to a single direct calculation of the moments of the exit time for all possible initial offsets. We have also confirmed that the simplified transport model used in the translocation calculation captures the behavior exhibited during more costly Brownian dynamics simulations. The results thus obtained indicate that the unhooking process is dominated by two regimes: (i) a purely convective regime, compatible with the deterministic model, and (ii) a "boundary layer" diffusion-dominated regime. The transition between the two regimes occurs at a critical offset of $N_c \sim 1/\sqrt{\mathrm{Pe}}$. When typical experimental values are considered, i.e., $N \sim 300$ and $\mathrm{Pe} \sim 0.1$, convective effects dominate and the chain unhooking process can be modeled in a deterministic way.

ACKNOWLEDGMENT

This work was supported in part by the David and Lucile Packard Foundation.

[1] J. L. Viovy, Rev. Mod. Phys. **72**, 813 (2000).
[2] C. Heller, T. A. J. Duke, and J. L. Viovy, Biopolymers **34**, 249 (1994).
[3] D. C. Schwartz and C. R. Cantor, Cell **37**, 67 (1984).
[4] G. W. Slater, S. Guillouzic, M. G. Gauthier, J. F. Mercier, M. Kenward, L. C. McCormick, and F. Tessier, Electrophoresis **23**, 3791 (2002).
[5] T. M. Squires and S. R. Quake, Rev. Mod. Phys. **77**, 977 (2005).
[6] R. B. Schoch, J. Han, and P. Renaud, Rev. Mod. Phys. **80**, 839 (2008).
[7] W. D. Volkmuth and R. H. Austin, Nature (London) **358**, 600 (1992).
[8] N. Kaji, Y. Tezuka, Y. Takamura, M. Ueda, T. Nishimoto, H. Nakanishi, Y. Horiike, and Y. Baba, Anal. Chem. **76**, 15 (2004).
[9] P. S. Doyle, J. Bibette, A. Bancaud, and J. L. Viovy, Science **295**, 2237 (2002).
[10] N. Minc, C. Fütterer, K. D. Dorfman, A. Bancaud, C. Gosse, C. Goubault, and J. L. Viovy, Anal. Chem. **76**, 3770 (2004).
[11] W. D. Volkmuth, T. A. J. Duke, M. C. Wu, R. H. Austin, and A. Szabo, Phys. Rev. Lett. **72**, 2117 (1994).
[12] G. I. Nixon and G. W. Slater, Phys. Rev. E **50**, 5033 (1994).
[13] N. Minc, J. L. Viovy, and K. D. Dorfman, Phys. Rev. Lett. **94**, 198105 (2005).
[14] G. C. Randall and P. S. Doyle, Macromolecules **38**, 2410 (2005).
[15] M. Kenward and G. W. Slater, Eur. Phys. J. E **20**, 125 (2006).
[16] E. M. Sevick and D. R. M. Williams, Eur. Phys. Lett. **56**, 529 (2001).
[17] J. M. Deutsch, Science **240**, 922 (1988).
[18] J. M. Deutsch and T. L. Madden, J. Chem. Phys. **90**, 2476

(1989).
[19] J. M. Deutsch, J. Chem. Phys. **90**, 7436 (1989).
[20] S. Popelka, Z. Kabatek, J. L. Viovy, and B. Gas, J. Chromatogr. A **838**, 45 (1999).
[21] K. D. Dorfman, Phys. Rev. E **73**, 061922 (2006).
[22] K. D. Dorfman, Phys. Rev. E **77**, 019901(E) (2008).
[23] A. Mohan and P. S. Doyle, Macromolecules **40**, 8794 (2007).
[24] W. Sung and P. J. Park, Phys. Rev. Lett. **77**, 783 (1996).
[25] M. Muthukumar, J. Chem. Phys. **111**, 10371 (1999).
[26] O. Flomenbom and J. Klafter, Phys. Rev. E **68**, 041910 (2003).
[27] M. G. Gauthier and G. W. Slater, J. Chem. Phys. **128**, 065103 (2008).
[28] J. M. Schurr and S. B. Smith, Biopolymers **29**, 1161 (1990).
[29] P. André, D. Long, and A. Ajdari, Eur. Phys. J. B **4**, 307 (1998).
[30] A. Szabo, K. Schulten, and Z. Schulten, J. Chem. Phys. **72**, 4350 (1980).
[31] M. G. Gauthier and G. W. Slater, Phys. Rev. E **70**, 015103(R) (2004).
[32] G. W. Slater, Electrophoresis **14**, 1 (1993).
[33] R. M. Mnatsakanov, Stat. Probab. Lett. **78**, 1869 (2008).
[34] J. M. Kim and P. S. Doyle, J. Chem. Phys. **125**, 074906 (2006).
[35] G. C. Randall and P. S. Doyle, Phys. Rev. Lett. **93**, 058102 (2004).
[36] R. M. Jendrejack, J. J. de Pablo, and M. D. Graham, J. Chem. Phys. **116**, 7752 (2002).
[37] J. F. Marko and E. D. Siggia, Macromolecules **28**, 8759 (1995).
[38] P. T. Underhill and P. S. Doyle, J. Non-Newtonian Fluid Mech. **122**, 3 (2004).
[39] D. M. Heyes and J. R. Melrose, J. Non-Newtonian Fluid Mech. **46**, 1 (1993).